JCI insight

Evofosfamide for the treatment of human papillomavirus-negative head and neck squamous cell carcinoma

Stephen M.F. Jamieson, … , Michael A. Curran, Francis W. Hunter

JCI Insight. 2018;3(16):e122204. https://doi.org/10.1172/jci.insight.122204.

Research Article | Oncology | Therapeutics

Evofosfamide (TH-302) is a clinical-stage hypoxia-activated prodrug of a DNA-crosslinking nitrogen mustard that has potential utility for human papillomavirus (HPV) negative head and neck squamous cell carcinoma (HNSCC), in which tumor hypoxia limits treatment outcome. We report the preclinical efficacy, target engagement, preliminary predictive biomarkers and initial clinical activity of evofosfamide for HPV-negative HNSCC. Evofosfamide was assessed in 22 genomically characterized cell lines and 7 cell line–derived xenograft (CDX), patient-derived xenograft (PDX), orthotopic, and syngeneic tumor models. Biomarker analysis used RNA sequencing, whole-exome sequencing, and whole-genome CRISPR knockout screens. Five advanced/metastatic HNSCC patients received evofosfamide monotherapy (480 mg/m^2 qw × 3 each month) in a phase 2 study. Evofosfamide was potent and highly selective for hypoxic HNSCC cells. Proliferative rate was a predominant evofosfamide sensitivity determinant and a proliferation metagene correlated with activity in CDX models. Evofosfamide showed efficacy as monotherapy and with radiotherapy in PDX models, augmented CTLA-4 blockade in syngeneic tumors, and reduced hypoxia in nodes disseminated from an orthotopic model. Of 5 advanced HNSCC patients treated with evofosfamide, 2 showed partial responses while 3 had stable disease. In conclusion, evofosfamide shows promising efficacy in aggressive HPV-negative HNSCC, with predictive biomarkers in development to support further clinical evaluation in this indication.

JCI insight

RESEARCH ARTICLE

Evofosfamide for the treatment of human papillomavirus-negative head and neck squamous cell carcinoma

Stephen M.F. Jamieson,[1,2,3] Peter Tsai,[4] Maria K. Kondratyev,[5] Pratha Budhani,[6] Arthur Liu,[6] Neil N. Senzer,[7] E. Gabriela Chiorean,[8,9] Shadia I. Jalal,[8] John J. Nemunaitis,[10] Dennis Kee,[11] Avik Shome,[1] Way W. Wong,[1] Dan Li,[1] Nooriyah Poonawala-Lohani,[12] Purvi M. Kakadia,[4] Nicholas S. Knowlton,[2,4] Courtney R.H. Lynch,[1] Cho R. Hong,[1] Tet Woo Lee,[1,2] Reidar A. Grénman,[13] Laura Caporiccio,[5] Trevor D. McKee,[14] Mark Zaidi,[5,14] Sehrish Butt,[14] Andrew M.J. Macann,[15] Nicholas P. McIvor,[16] John M. Chaplin,[16] Kevin O. Hicks,[1,2] Stefan K. Bohlander,[2,4] Bradly G. Wouters,[5,17,18] Charles P. Hart,[19] Cristin G. Print,[2,4] William R. Wilson,[1,2] Michael A. Curran,[6] and Francis W. Hunter[1,2]

[1]Auckland Cancer Society Research Centre, University of Auckland, Auckland, New Zealand. [2]Maurice Wilkins Centre for Molecular Biodiscovery, University of Auckland, Auckland, New Zealand. [3]Department of Pharmacology and Clinical Pharmacology, University of Auckland, Auckland, New Zealand. [4]Department of Molecular Medicine and Pathology, University of Auckland, Auckland, New Zealand. [5]Princess Margaret Cancer Centre, University Health Network, Toronto, Ontario, Canada. [6]Department of Immunology, University of Texas, MD Anderson Cancer Center, Houston, Texas, USA. [7]Mary Crowley Cancer Research Center, Dallas, Texas, USA. [8]Indiana University Melvin and Bren Simon Cancer Center, Indiana University, Indianapolis, Indiana, USA. [9]Fred Hutchinson Cancer Research Center, University of Washington, Seattle, Washington, USA. [10]Department of Medicine, University of Toledo College of Medicine and Life Sciences, University of Toledo, Toledo, Ohio, USA. [11]LabPLUS, Auckland City Hospital, Auckland, New Zealand. [12]The Bioinformatics Institute, University of Auckland, Auckland, New Zealand. [13]Department of Otolaryngology–Head and Neck Surgery, Turku University Hospital, Turku, Finland. [14]STTARR Innovation Centre, University Health Network, Toronto, Ontario, Canada. [15]Department of Radiation Oncology, Auckland City Hospital, Auckland, New Zealand. [16]Department of Otolaryngology–Head and Neck Surgery, Auckland City Hospital, Auckland, New Zealand. [17]Department of Radiation Oncology, University of Toronto, Toronto, Ontario, Canada. [18]Department of Medical Biophysics, University of Toronto, Toronto, Ontario, Canada. [19]Threshold Pharmaceuticals, South San Francisco, California, USA.

Evofosfamide (TH-302) is a clinical-stage hypoxia-activated prodrug of a DNA-crosslinking nitrogen mustard that has potential utility for human papillomavirus (HPV) negative head and neck squamous cell carcinoma (HNSCC), in which tumor hypoxia limits treatment outcome. We report the preclinical efficacy, target engagement, preliminary predictive biomarkers and initial clinical activity of evofosfamide for HPV-negative HNSCC. Evofosfamide was assessed in 22 genomically characterized cell lines and 7 cell line–derived xenograft (CDX), patient-derived xenograft (PDX), orthotopic, and syngeneic tumor models. Biomarker analysis used RNA sequencing, whole-exome sequencing, and whole-genome CRISPR knockout screens. Five advanced/metastatic HNSCC patients received evofosfamide monotherapy (480 mg/m^2 qw × 3 each month) in a phase 2 study. Evofosfamide was potent and highly selective for hypoxic HNSCC cells. Proliferative rate was a predominant evofosfamide sensitivity determinant and a proliferation metagene correlated with activity in CDX models. Evofosfamide showed efficacy as monotherapy and with radiotherapy in PDX models, augmented CTLA-4 blockade in syngeneic tumors, and reduced hypoxia in nodes disseminated from an orthotopic model. Of 5 advanced HNSCC patients treated with evofosfamide, 2 showed partial responses while 3 had stable disease. In conclusion, evofosfamide shows promising efficacy in aggressive HPV-negative HNSCC, with predictive biomarkers in development to support further clinical evaluation in this indication.

Conflict of interest: SMJ and WRW are named as inventors on a patent (US9101632B2) relating to the clinical-stage hypoxia-targeting prodrug tarloxotinib bromide. MAC has stock or other ownership interests in Oncoresponse, ImmunOS, Esperion, Molecular Templates and CytomX. MAC received honoraria from Pfizer and Amgen. MAC has consulting or advisory roles with ImmunoMet, ImmunOS, Innovio, Agenus, Nurix, Aptevo, Xencor, and Pieris. MAC received research funding from AstraZeneca and ImmunoMet. EGC received research funding from Celgene, Incyte, Igynta, Stemline, Boehringer-Ingelheim, Lily, and Merck. EGC has Advisory Board roles for Celgene, Vicus Therapeutics, Five Prime, Halozyme, Genentech, NovoCure, Merrimack, and Pfizer. SIJ received research funding from AstraZeneca. CGP is on the Board of Directors of the New Zealand Institute of Environmental Science and Research, which has interests in human health diagnostics. CPH was an employee and stockholder of Threshold Pharmaceuticals (now Molecular Templates), the developer of evofosfamide.

Submitted: May 14, 2018
Accepted: July 13, 2018
Published: August 23, 2018

Reference information:
JCI Insight. 2018;3(16):e122204.
https://doi.org/10.1172/jci.insight.122204.

Introduction

Hypoxia has been explored as a therapeutic target due to its prevalence and severity in tumors and its contributions to aggressive disease (1). The evidence supporting hypoxia as an oncology target is strongest in head and neck squamous cell carcinoma (HNSCC) (2–4), a malignancy that accounts for 5% of global cancer mortality (5). Risk of HNSCC is strongly linked to tobacco and alcohol exposure (6) and infection with high-risk human papillomavirus (HPV) serotypes (7). HPV-associated disease represents a distinct entity with a lower mutational burden (8, 9), greater lymphocytic and myeloid infiltration (10), and favorable prognosis (11, 12). Locally advanced HNSCC is treated with surgery and definitive radiotherapy, often with concurrent platinum-based chemotherapy (13, 14). Overexpression of the epidermal growth factor receptor (EGFR) in a subset of tumors (15) led to the development of cetuximab with radiotherapy for locally advanced HNSCC (16) and with chemotherapy at first-line for metastatic/recurrent disease (17). Immunotherapy has also shown efficacy for HNSCC (18, 19), with nivolumab and pembrolizumab both approved at second-line for recurrent/metastatic HNSCC, though response rates to anti–PD-1 monotherapy remain disappointing at 15%.

These advances notwithstanding, HNSCC survival has not markedly improved in recent decades and distant metastasis, locoregional recurrence, second primaries, and therapy resistance remain major challenges. Hypoxia is a marker of poor prognosis (3) and predictor of radiotherapy failure in HNSCC (2), specifically in HPV-negative disease (4). Accordingly, a voluminous literature has investigated hypoxic modification to improve HNSCC outcomes (20). Notable approaches include modified oxygen breathing (21), oxygen-mimetic radiosensitizers (22), and direct ablation of hypoxic cells with selective cytotoxins (23), though such strategies have not seen widespread adoption. Compelling evidence also points to a role for hypoxia in immune evasion (24). Hypoxia-inducible factor 1 (HIF-1) is a transcriptional activator of PD-L1 in myeloid and tumor cells (25) and HIF transcriptional signatures inversely correlate with T cell infiltration in HNSCC (26). Hypoxia promotes the recruitment of regulatory T cells (27, 28) and tumor-associated macrophages (TAMs) (29), production of PGE_2, IL-6, and IL-10 (30), and the immunosuppressive activity of myeloid cells (31, 32). Additionally, hypoxia results in extracellular accumulation of adenosine and impairment of T cell–mediated immunity (33). Extracellular acidification associated with hypoxic microenvironments also creates a formidable barrier to T cell function and persistence (34–36).

Such considerations highlight the rationale for targeting hypoxia in HNSCC, both in the context of radiation oncology for local disease and with T cell–directed immunotherapies for advanced disease. Evofosfamide is a clinical-stage hypoxia-activated prodrug designed to target the DNA-crosslinking nitrogen mustard bromo-*iso*-phosphoramide (Br-IPM) to regions of hypoxia (37), leading to DNA damage, γH2AX phosphorylation, cell cycle arrest, and cleavage of caspase-3 and -6 (38–40). Despite narrowly missing its primary phase 3 overall survival (OS) endpoint with gemcitabine for advanced pancreatic adenocarcinoma (41), evofosfamide shows abundant evidence of preclinical (40, 42–51) and clinical activity (52, 53). However, evofosfamide has not been comprehensively investigated for HNSCC. Here, we report the preclinical efficacy, target engagement, development of predictive biomarkers, and initial clinical activity of evofosfamide for this indication.

Results

Evofosfamide is potent and highly selective for hypoxic HNSCC cells. To explore the potential of evofosfamide for HNSCC, we assembled 27 HPV-negative cell lines derived from HNSCC of varying primary site, histopathological grade, and TNM stage (Table 1) and characterized 22 of these by whole-exome sequencing (Supplemental File 1; supplemental material available online with this article; https://doi.org/10.1172/jci.insight.122204DS1). In a subset of cases, paired cell lines isolated from primary, nodal, and/or recurrent sites in the same patient were studied. We compared the in vitro antiproliferative potency and hypoxic selectivity of evofosfamide to other hypoxia-activated prodrugs PR-104A (54) and SN30000 (55) (Supplemental Figure 1). We also compared Br-IPM, the active metabolite of evofosfamide, to the standard chemotherapy agents cisplatin and 5-fluorouracil (Supplemental Figure 2). This study examined 21 HNSCC cell lines challenged with compounds under anoxia (N_2) or 20% oxygen (henceforth referred to as Air, see Figure 1A for structures and Supplemental File 2 for the full dataset) to define IC_{50} values (drug concentrations for 50% inhibition of cell growth). Evofosfamide showed nanomolar potency for HNSCC cells under anoxia and was strongly suppressed by oxygen, with a median Air/N_2 IC_{50} ratio of 360-fold (Figure 1B). Evofosfamide was significantly more potent and selective than PR-104A or SN30000 (Figure 1C) and was

Table 1. Characteristics of the human HNSCC cell lines used in this study and their source tumors

Designation[A]	Primary Site	Type	Stage[B]	Grade[B]	DNA ploidy[C]
FaDu	Hypopharynx	Primary	-	-	-
SCC-4	Lingus	Primary	-	-	5.69 (100)
SCC-9	Lingus	Primary	-	-	2.88 (100)
UT-SCC-1A	Gingiva	Primary	$T_2N_1M_0$	I	2.1 (100)
UT-SCC-1B	Gingiva	Recurrence			2.0 (92), 3.1 (8)
UT-SCC-16A	Lingus	Primary	$T_3N_0M_0$	III	1.8 (100)
UT-SCC-16B	Lingus	Nodal			4.2 (100)
UT-SCC-19A	Glottic larynx	Primary	$T_4N_0M_0$	II	2.8 (70), 3.8 (30)
UT-SCC-19B	Glottic larynx	Recurrence			2.4 (100)
UT-SCC-24A	Lingus	Primary	$T_2N_0M_0$	II	3.5 (100)
UT-SCC-42A	Supraglottic larynx	Primary	$T_4N_3M_0$	III	3.4 (100)
UT-SCC-42B	Supraglottic larynx	Nodal			3.3 (100)
UT-SCC-46A	Gingiva; maxilla	Primary	$T_1N_0M_0$	I	2.1 (100)
UT-SCC-54A	Buccal mucosa	Primary	$T_2N_0M_0$	I	3.6 (97), 1.8 (3)
UT-SCC-54B	Buccal mucosa	Recurrence			3.7 (98), 1.9 (2)
UT-SCC-54C	Buccal mucosa	Nodal			2.0 (100)
UT-SCC-59C	Parotid	Nodal	$T_1N_3M_0$	III	-
UT-SCC-60A	Tonsilla	Primary	$T_4N_1M_0$	I	3.2 (100)
UT-SCC-63A	Gingiva; mandibula	Primary	$T_4N_0M_0$	I	1.9 (50), 3.6 (50)
UT-SCC-74A	Lingus	Primary	$T_3N_1M_0$	II	3.8 (100)
UT-SCC-74B	Lingus	Nodal			2.7 (85), 2.0 (15)
UT-SCC-76A	Lingus	Primary	$T_3N_0M_0$	II	3.2 (100)
UT-SCC-76B	Lingus	Recurrence			3.4 (100)
UT-SCC-79A	Parotid	Nodal	$T_XN_{2b}M_0$	II	3.5 (100)
UT-SCC-110A	Gingiva; maxillary sinus	Recurrence	$T_4N_0M_0$	III	2.7 (100)
UT-SCC-110B	Gingiva; maxillary sinus	Nodal			3.1 (100)
UT-SCC-126A	Labii inferioris	Primary	$T_2N_1M_0$	I	4.2 (53), 3.7 (43), 1.9 (4)

[A]Cell lines with the same numeric designation were isolated from a single patient. [B]Staging and histopathological grade at first diagnosis. [C]DNA content of cell lines as determined by flow cytometric analysis of propidium iodide–stained cells. Values in parentheses denote the percentage of totals cells with a given DNA content.

equivalently active against lines derived from primary, nodal, or recurrent lesions (Figure 1D). Cell line sensitivity to evofosfamide was strongly correlated with sensitivity to Br-IPM under anoxia and weakly correlated with cisplatin but not with other agents (Figure 1E), in keeping with a DNA-crosslinking mechanism of action for evofosfamide and suggesting that variation in the intrinsic sensitivity of HNSCC cell lines to Br-IPM accounts for a significant component of the 19-fold spread in anoxic IC_{50} values for evofosfamide. To investigate this further, we measured the reductive activation of evofosfamide (see Figure 2A for the metabolic pathway) by liquid chromatography–tandem mass spectrometry (LC–MS/MS) in 15 cell lines (Figure 2B). Evofosfamide activation rates were variable between cell lines and combining reductive activation (measured as the concentration of metabolites produced) with Br-IPM sensitivity (anoxic IC_{50}) as independent variables in a multiple linear regression model — $\log_{10}(\text{evofosfamide } IC_{50}) = a + (b \times \log_{10}[\text{Br-IPM } IC_{50}]) + (c \times \log_{10}[\text{Br-IPM + Cl-IPM concentration}])$ — improved the fit between predicted and measured evofosfamide IC_{50} from R = 0.73 to R = 0.85 (Figure 2C and Supplemental Table 1). These data confirmed that evofosfamide responsiveness is significantly determined by sensitivity to DNA crosslinking, with the rate of evofosfamide activation serving as an additional determinant.

A proliferation metagene correlates with evofosfamide sensitivity. To explore molecular correlates of evofosfamide sensitivity, we performed RNA sequencing (RNAseq) on the HNSCC cell lines (Supplemental Figure 3) and differential expression analysis of evofosfamide-sensitive and -resistant lines dichotomized by the arithmetic mean anoxic IC_{50} value (Figure 3A), defining genes differentially expressed in evofosfamide-sensitive and -resistant cell lines (Figure 3B and Supplemental File 3). Querying the latter for enrichments of gene ontology and pathway classifiers identified overrepresentation of terms relating to the cell cycle (Benjamini-Hochberg–adjusted Fisher's exact *P* value, false discovery rate [FDR] < 10^{-12}), DNA repair (FDR < 10^{-10}), and

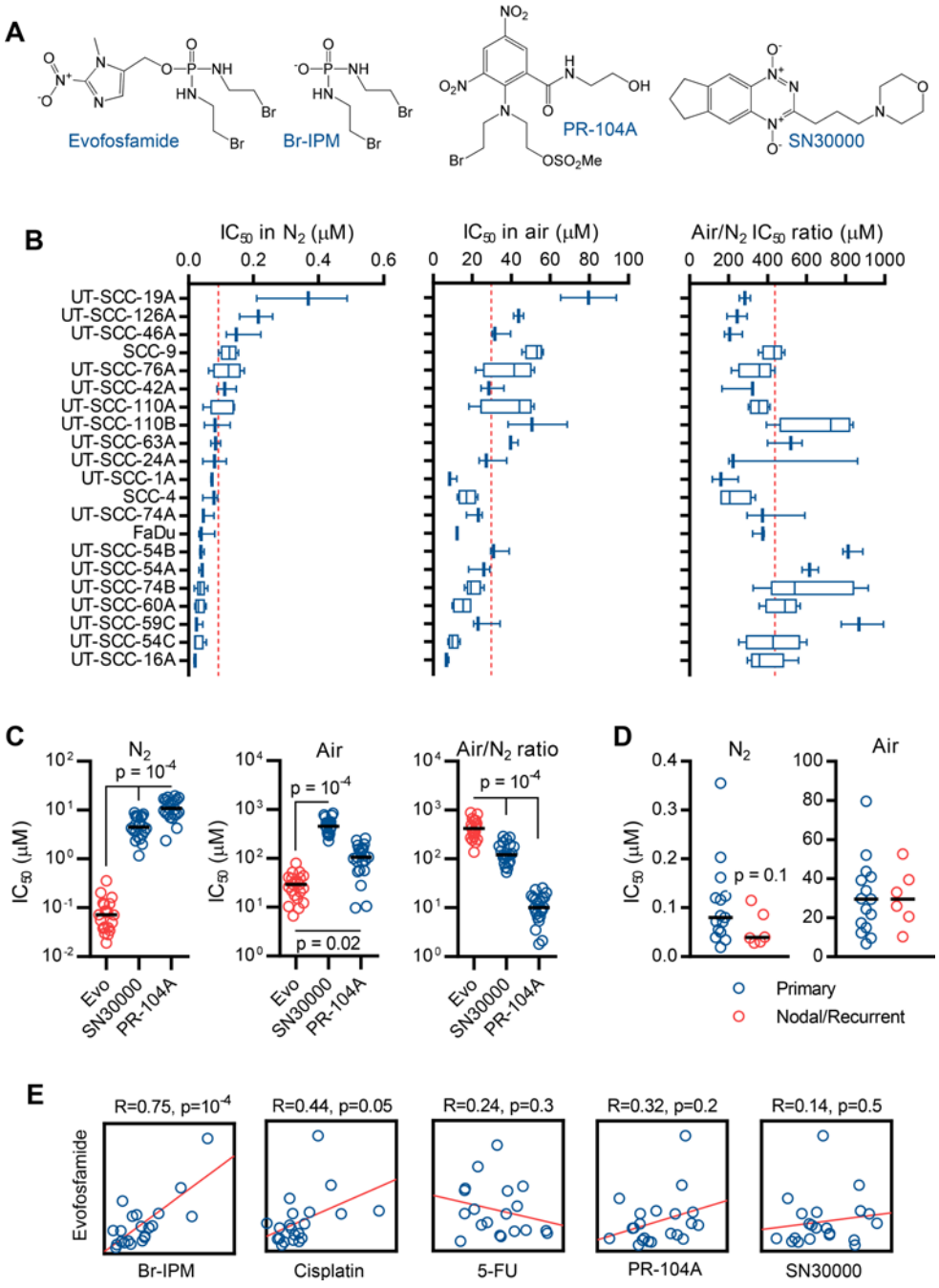

Figure 1. Potency and hypoxic selectivity of evofosfamide and reference agents for head and neck squamous cell carcinoma (HNSCC) cell lines. (**A**) Chemical structures of evofosfamide, its DNA crosslinking metabolite bromo-*iso*-phosphoramide mustard (Br-IPM), and the comparator hypoxia-activated prodrugs PR-104A (a dinitrobenzamide) and SN30000 (a benzotriazine di-*N*-oxide). (**B**) Antiproliferative activity of evofosfamide – measured as the concentration required for 50% inhibition of cell growth (IC_{50}) – in 21 HNSCC cell lines assessed by sulforhodamine B assay after 4-hour drug exposure under anoxia (N_2) or ambient oxygen (air) followed by 5-day regrowth, with hypoxia selectivity represented as the Air-N_2 IC_{50} quotient. The Air/N_2 ratio is plotted as the mean ± SEM from 3 or more intraexperiment quotients calculated from anoxic and normoxic assays performed on the same days. Boxes represent the median and interquartile range, whereas whiskers mark the minimum and maximum IC_{50} determinations from 3 or more independent experiments. Dashed lines denote the mean IC_{50} values for the cell line panel. (**C**) Comparison of the in vitro antiproliferative potency and hypoxic selectivity of evofosfamide (evo), PR-104A, and SN30000 in 21 HNSCC cell lines. Data points denote mean IC_{50} values for individual cell lines computed from 3 or more experiments, with IC_{50} values and Air/N_2 IC_{50} quotients defined as per panel **B**. Horizontal lines mark the median values. The statistical significance of differences in the potency and selectivity of drugs was assessed by 1-way ANOVA with Dunnett's correction. (**D**) Comparison of the antiproliferative potency (as IC_{50} under N_2 or air) of evofosfamide in HNSCC cell lines derived from primary (n = 15) or nodal/recurrent (n = 6) lesions. Statistical significance of differences in IC_{50} values between these groups was assessed by Mann-Whitney test. (**E**) Comparison of the pattern of HNSCC cell line sensitivity (as IC_{50} values) to evofosfamide and to Br-IPM, cisplatin, 5-FU, PR-104A, and SN30000 under anoxia. IC_{50} values were defined as per panel **B** and data points correspond to individual cell lines. Axes are linear and functions are Pearson's correlations.

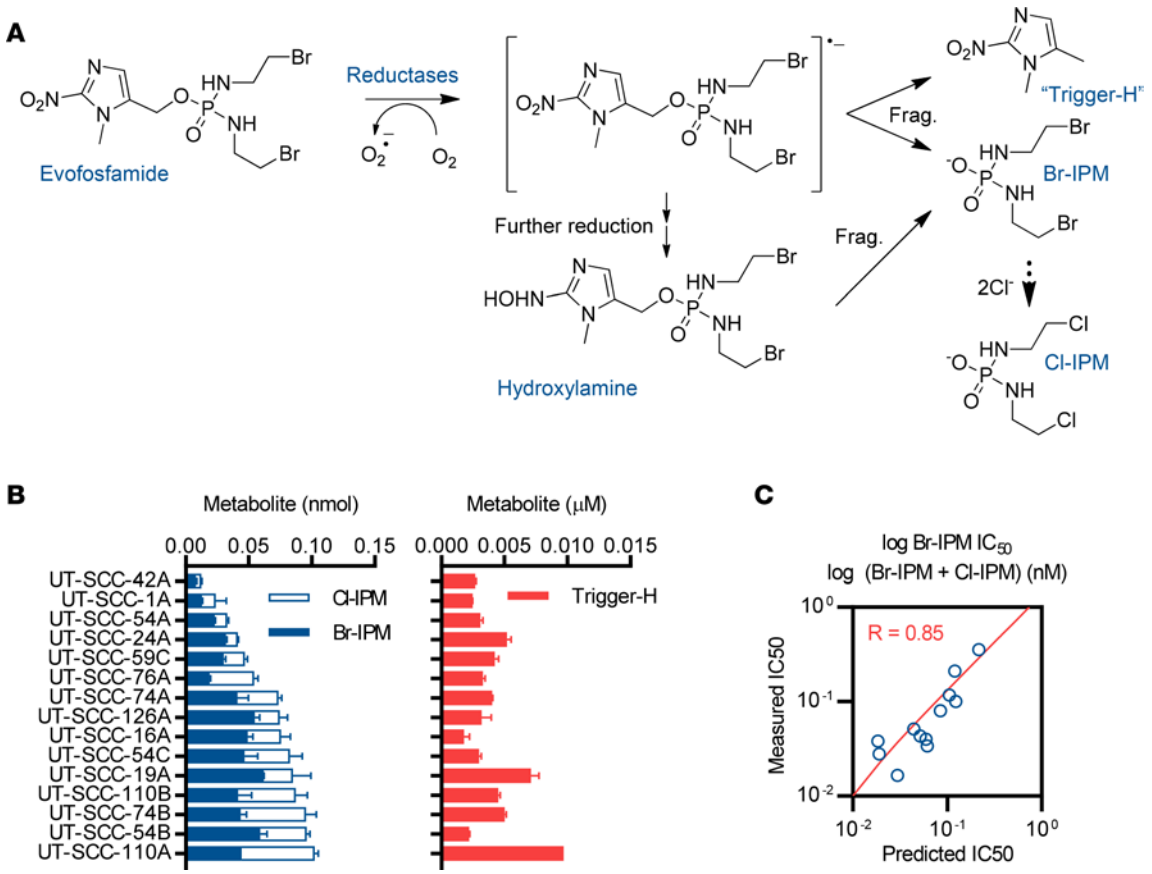

Figure 2. Enzymatic activation of evofosfamide and its contribution to antiproliferative activity in a subset of 15 cultured head and neck squamous cell carcinoma (HNSCC) cell lines. (**A**) Route of metabolic activation of evofosfamide in hypoxic tumor cells by enzymatic 1-electron reduction. As described in literature (39), evofosfamide undergoes enzyme-catalyzed 1-electron reduction to a transient radical anion that fragments to release Br-IPM and the free 2-nitroimidazole trigger ("Trigger-H"). In the presence of oxygen, the radical anion is back-oxidized to evofosfamide, preventing accumulation of Br-IPM and thus conferring hypoxic selectivity. Fragmentation at the 1-electron (radical anion) stage competes with further reduction to the corresponding hydroxylamine, which also fragments to release Br-IPM but does not generate Trigger-H. Halide exchange results in the conversion of Br-IPM to more stable Cl-IPM. Br-IPM, Cl-IPM, and Trigger-H are thus all diagnostic of the reductive activation of evofosfamide. Frag, fragmentation. (**B**) Comparison of the facility of reductive activation of evofosfamide in HNSCC cell lines by liquid chromatography–tandem mass spectrometry (LC-MS/MS) measurement of intracellular Br-IPM, Cl-IPM, and Trigger-H concentrations at the endpoint of 1-hour exposures to 30 μM evofosfamide under anoxia. Data are the mean ± range from 2 independent determinations. (**C**) Multiple linear regression of measured evofosfamide antiproliferative activity (as the concentration required for 50% inhibition of cell growth, IC_{50}) in 15 HNSCC cell lines under anoxia compared to IC_{50} values predicted in the same lines using log Br-IPM IC_{50} under anoxia as a measure of sensitivity to the active metabolite and the log of the sum of the intracellular concentrations of Br-IPM and Cl-IPM formed from evofosfamide (i.e., the values plotted in panel **B**) as a measure of its reductive metabolism.

DNA metabolism (FDR < 10^{-18}; Figure 3C). This result was reproduced when cell lines were dichotomized by the geometric mean IC_{50} value or separated into tertiles (not shown). Related terms were similarly enriched among genes that correlated with evofosfamide sensitivity when anoxic IC_{50} values were treated as a continuous variable (Supplemental Figure 4). As an orthogonal approach, we performed whole-genome CRISPR knockout screens in UT-SCC-74B cells transduced with the GeCKOv2 single guide RNA (sgRNA) library (56). Cas9-expressing UT-SCC-74B cells were transduced to generate a knockout library that was highly complex (Supplemental Figure 5, A–C) and functionally validated by screening with 6-thioguanine, where drug exposure resulted in outgrowth of cells carrying mutations in the known 6-thioguanine sensitivity genes *HPRT1* and *NUDT5* (Supplemental Figure 5, D and E). Challenging this library separately with evofosfamide and Br-IPM (Figure 4A) selected for differential survival of clones carrying sgRNA targeted to putative modifiers of drug sensitivity (Figure 4B). Functional analysis of the latter revealed overrepresentation of genes involved in cell proliferation (gene ontology classifier GO0042127; FDR < 0.05). To develop an initial predictive biomarker for evofosfamide from these findings, we hierarchically clustered the HNSCC cell lines using a published (57) 61-gene proliferation signature — 49 of which were expressed in the cell lines (Supplemental File 4) — to define proliferation^{lo} and proliferation^{hi} classes (Figure 4C). The proliferation^{lo} and proliferation^{hi}

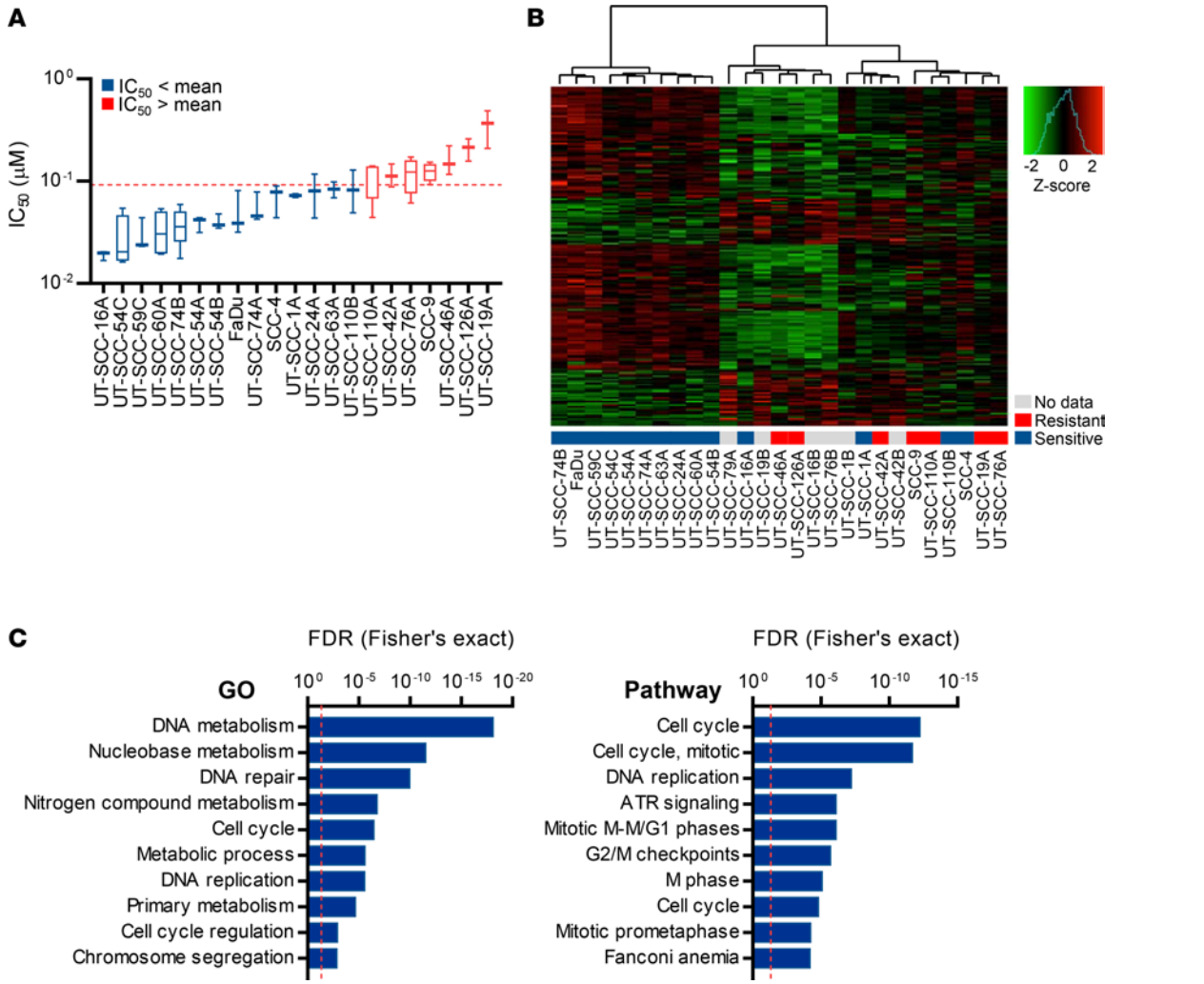

Figure 3. Sensitivity of HNSCC cell lines to evofosfamide is associated with expression of proliferation-related genes. (**A**) Head and neck squamous cell carcinoma (HNSCC) cell lines dichotomized by the arithmetic mean of anoxic evofosfamide IC_{50} values into sensitive and resistant groups for differential expression analysis using RNA sequencing. Data are defined as in Figure 1B. (**B**) Unsupervised hierarchical clustering of HNSCC cell lines according to their expression of the top 200 most differentially expressed genes (by *P* value) between evofosfamide-sensitive and evofosfamide-resistant cell lines. The gene list was defined using *limma* and the clustering performed using the ward.D method with Euclidean distance. (**C**) Statistical overrepresentation of gene ontology (GO) terms (assessed using PANTHER [ref. 80]; left) or molecular pathways (assessed using GeneSetDB [ref. 81], right) among the 200 genes most differentially expressed between evofosfamide-sensitive and evofosfamide-resistant cell lines (as per panel **B**). False discovery rates (FDRs) arising from Benjamini–Hochberg adjustment of *P* values from Fisher's exact tests are shown for the 10 most significant GO and pathway findings. Dashed lines denote the 5% FDR.

classes showed differential population doubling times (Supplemental Figure 6) and in vitro sensitivity to evofosfamide (Figure 4D), with rapidly proliferating lines more susceptible to treatment.

Evofosfamide is active against biomarker-selected HNSCC cell line–derived xenograft models. We compared the efficacy of evofosfamide monotherapy or in combination with radiotherapy in CDX models predicted to be differentially sensitive by biomarker analysis. UT-SCC-54C xenografts (proliferation^{hi}) were highly hypoxic, with a pimonidazole-positive fraction of 13% ± 0.6% (mean ± SEM, $n = 4$), while tumors grown from proliferation^{lo} UT-SCC-110B cells were less hypoxic (3.7% ± 0.4%, $n = 4$). Despite having limited monotherapy activity in UT-SCC-54C, evofosfamide slowed median tumor growth when administered concurrently with radiotherapy and significantly prolonged the time to 4-fold increase in tumor volume (RTV^4 44 vs. 31 days; log-rank $P = 0.003$, hazard ratio [HR] = 0.3 vs. radiotherapy; Figure 5A). The addition of evofosfamide to radiotherapy offered no additional benefit in the UT-SCC-110B model predicted to be treatment refractory (Figure 5B).

Evofosfamide is active against HNSCC patient–derived xenograft models. Next, we evaluated the activity of evofosfamide in 3 patient-derived xenograft (PDX) models derived from laryngeal and lingual squamous cell carcinomas (Figure 6; see supplement section 4 for clinical history and histopathology). In all cases, the histol-

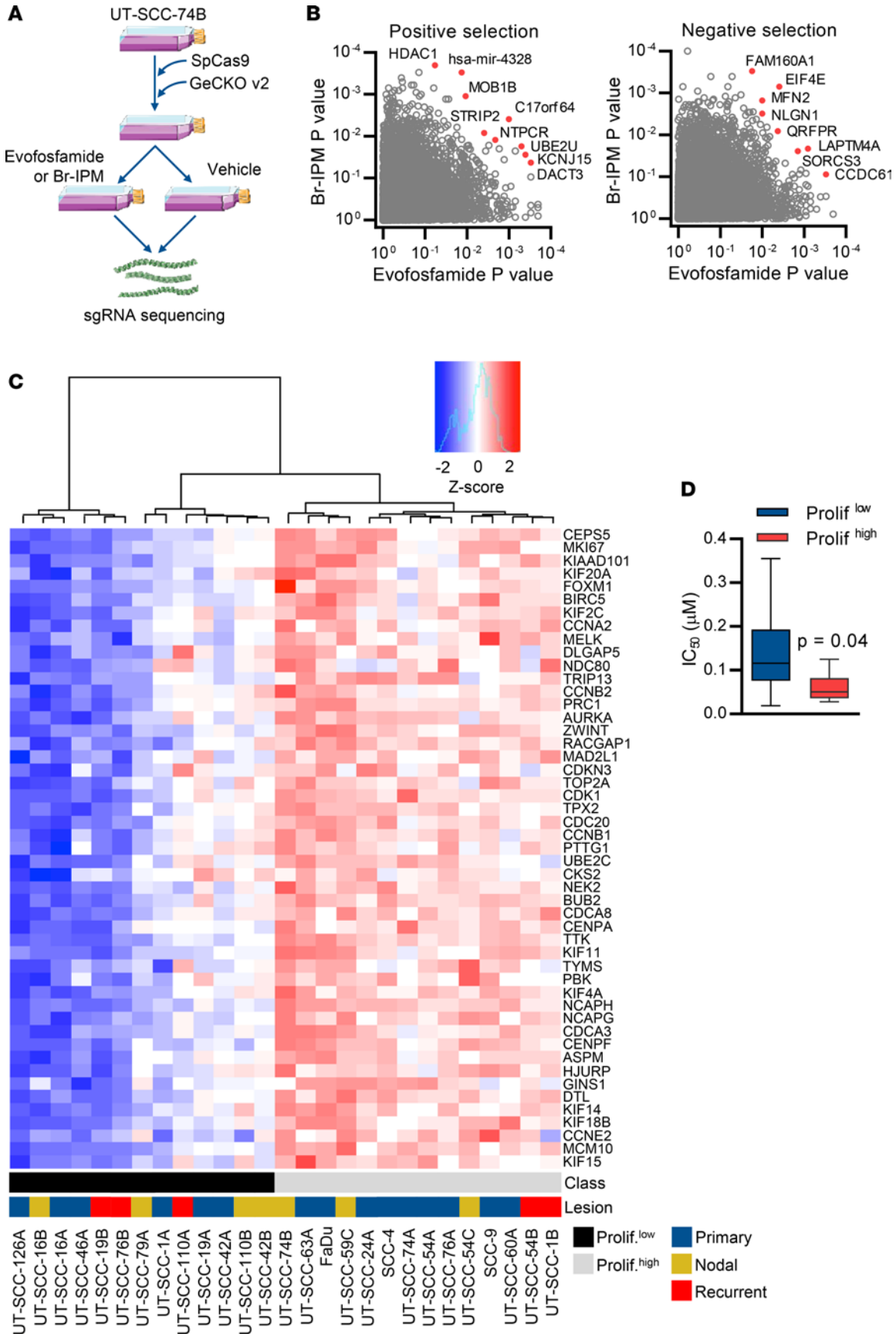
A
UT-SCC-74B
SpCas9
GeCKO v2
Evofosfamide
or Br-IPM
Vehicle
sgRNA sequencing
B
Positive selection
HDAC1
hsa-mir-4328
MOB1B
STRIP2
C17orf64
NTPCR
UBE2U
KCNJ15
DACT3
Br-IPM P value
Evofosfamide P value
Negative selection
FAM160A1
EIF4E
MFN2
NLGN1
QRFPR
LAPTM4A
SORCS3
CCDC61
C
-2 0 2
Z-score
CEPS5
MKI67
KIAAD101
KIF20A
FOXM1
BIRC5
KIF2C
CCNA2
MELK
DLGAP5
NDC80
TRIP13
CCNB2
PRC1
AURKA
ZWINT
RACGAP1
MAD2L1
CDKN3
TOP2A
CDK1
TPX2
CDC20
CCNB1
PTTG1
UBE2C
CKS2
NEK2
BUB2
CDCA8
CENPA
TTK
KIF11
TYMS
PBK
KIF4A
NCAPH
NCAPG
CDCA3
CENPF
ASPM
HJURP
GINS1
DTL
KIF14
KIF18B
CCNE2
MCM10
KIF15
Class
Lesion
UT-SCC-126A
UT-SCC-16B
UT-SCC-16A
UT-SCC-46A
UT-SCC-19B
UT-SCC-76B
UT-SCC-79A
UT-SCC-1A
UT-SCC-110A
UT-SCC-19A
UT-SCC-42A
UT-SCC-110B
UT-SCC-42B
UT-SCC-74B
UT-SCC-63A
FaDu
UT-SCC-59C
UT-SCC-24A
SCC-4
UT-SCC-74A
UT-SCC-54A
UT-SCC-76A
UT-SCC-54C
SCC-9
UT-SCC-60A
UT-SCC-54B
UT-SCC-1B
Prolif.low
Prolif.high
Primary
Nodal
Recurrent
D
Prolif low
Prolif high
IC50 (μM)
p = 0.04

Figure 4. A proliferation expression signature correlates with evofosfamide sensitivity in head and neck squamous cell carcinoma (HNSCC) cell lines. (**A**) The workflow for functional genomic screens for modifiers of evofosfamide or Br-IPM sensitivity. SpCas9, *Streptococcus pyogenes* Cas9. (**B**) Enrichment (positive selection) or depletion (negative selection) of single guide RNA (sgRNA) in evofosfamide- and Br-IPM-treated UT-SCC-74B cells (2 replicates per condition). The screen was deconvoluted using the RIGER method (83) with weighted-sum aggregation to output gene-level *P* values that were adjusted using the Benjamini-Hochberg method. (**C**) Unsupervised hierarchical clustering (ward.D method with Euclidean distance) of HNSCC cell lines according to their expression (measured by RNAseq) of a published tumor proliferation metagene (57). Of 61 genes in the proliferation cluster, 49 were expressed in HNSCC cells. The resulting proliferation metagene class assignments and whether cell lines were derived from primary, nodal, or recurrent lesions are indicated. (**D**) Differential in vitro sensitivity to evofosfamide per antiproliferative IC_{50} assay in HNSCC cell lines separated by proliferation metagene status, where the grouping of cell lines as proliferation^{hi} or proliferation^{lo} was accomplished by assignment of cell lines to binary clusters defined by unsupervised hierarchical clustering according to expression values of the metagene as shown in **C**. Box plots show the mean and interquartile range, whereas whiskers show the maximum and minimum IC_{50} values for metagene-high (n = 13) and metagene-low (n = 8) cell lines (≥3 independent experiments). Statistical significance was assessed by Mann–Whitney test.

ogy of the PDX tumors closely resembled the original clinical specimen (not shown). The PDX models all had inactivating missense mutations in *TP53*, while ACS-HN07 was a *PIK3CA*^{E545K} mutant and ACS-HN08 an *HRAS*^{G13V} and *NOTCH1*^{C1536Y} mutant (Supplemental Table 2). The pimonidazole-positive hypoxic fractions of the PDX models were 4.5% ± 0.5% (n = 7), 2.5% ± 0.5% (n = 4), and 3.0% ± 0.6% (n = 5) for ACS-HN06, ACS-HN07, and ACS-HN08, respectively. Evofosfamide monotherapy significantly prolonged survival in 2 PDX models (ACS-HN06: median time to RTV^4 29 vs. 18 days, log-rank P = 0.001, HR = 0.13; ACS-HN08: median time to RTV^4 undefined vs. 17 days, log-rank P = 0.03, HR = 0.34), with the least proliferative and hypoxic model, ACS-HN07, not achieving statistical significance for survival (median time to RTV^4 181 vs. 112 days, log-rank P = 0.08, HR = 0.18). In combination with radiotherapy, evofosfamide significantly prolonged survival in ACS-HN08 versus radiation alone (median time to RTV^4 50 vs. 10 days, log-rank P = 0.001, HR = 0.23), but provided no additional benefit to radiotherapy in ACS-HN06.

Evofosfamide reduces nodal hypoxia and augments CTLA-4 blockade. As clinical testing of evofosfamide would initially be for advanced HNSCC, we evaluated target engagement (as a reduction in hypoxic fraction) in spontaneously disseminated nodal metastases in an orthotopic UT-SCC-74B model (Figure 7A). Evofosfamide as monotherapy or with concurrent image-guided cervical node irradiation reduced the fraction of cytokeratin-positive tumor cells showing medium or high immunostaining for carbonic anhydrase 9 (CA9; Figure 7, B and C), an endogenous marker of hypoxia, consistent with target engagement in regionally metastatic disease.

Given the increasing use of immunotherapy for advanced HNSCC (18, 19) and the potential contributions of hypoxia to immunotherapy resistance (24), we evaluated evofosfamide in combination with CTLA-4 blockade in the syngeneic SCC-7 model, which was refractory to PD-1 blockade (not shown). Evofosfamide and anti–CTLA-4 antibody both moderately prolonged survival as single agents (Figure 7D; log-rank for evofosfamide P = 0.002, HR = 0.3; for anti–CTLA-4, P = 0.003, HR = 0.3), whereas concurrent combination therapy further improved survival (log-rank vs. anti–CTLA-4 alone, P = 0.01, HR = 0.3). These data highlighted the potential of combining evofosfamide with T cell–directed therapies for advanced HNSCC.

Evofosfamide shows initial evidence of activity in heavily pretreated HNSCC. We undertook initial clinical testing of evofosfamide for HNSCC as part of a phase 2 solid tumor expansion cohort to a previously published (52) phase 1a monotherapy trial (Supplemental Figure 7, NCT00495144). The phase 2 component of the study enrolled 72 subjects, including 5 with histologically confirmed locally advanced or metastatic HNSCC who had failed standard-of-care, including surgery and radiotherapy with concurrent cisplatin or cetuximab. These patients received single-agent evofosfamide by i.v. infusion at the recommended phase 2 dose of 480 mg/m^2 qw × 3 (1-week rest) for up to 6 cycles or until progression. Of the 5 HNSCC patients treated, 2 showed confirmed partial responses per Response Evaluation Criteria In Solid Tumors (RECIST) 1.0 lasting 113 and more than 176 days, while 3 had stable disease for a disease-control rate of 100%. Median progression-free survival (PFS) was 169 days (range 113 to 314 days), while median OS was not reached (range >113 to >316 days) after 316-day maximum follow-up. Safety was consistent with previous reports (52), with adverse events including nausea, skin rash fatigue, and emesis. A presented case study of a 71-year-old white female with poorly differentiated neck and oral cavity squamous cell carcinoma locally recurrent after prior surgery, radiotherapy, and cetuximab showed an excellent partial response of bulky disease at cycle 2 (Figure 8), which was maintained at cycle 4 prior to target lesion progression at cycle 6.

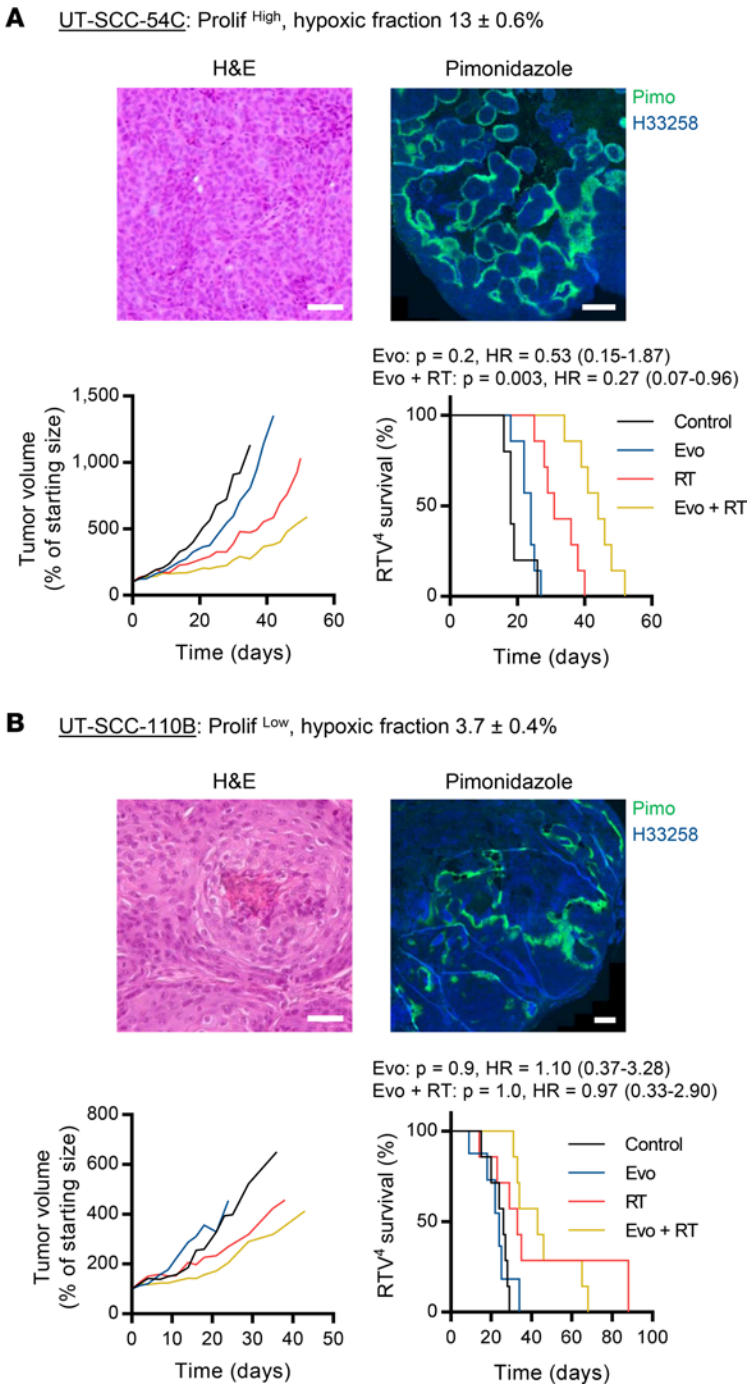

Figure 5. Efficacy of evofosfamide alone or with radiotherapy in biomarker-selected head and neck squamous cell carcinoma (HNSCC) cell line–derived xenograft models. Evofosfamide (evo) was assessed as a single agent (50 mg/kg i.p. qd × 5 weekly for 3 cycles) or in combination with radiotherapy (RT, 1 × 10 Gy on day 5 of the first cycle) by growth delay in the proliferation metagene-high, highly hypoxic cell line–derived xenograft (CDX) UT-SCC-54C (**A**) and the metagene-low, less hypoxic CDX UT-SCC-110B (**B**). Growth plots show the volume of the median tumor at each assessment. Survival analyses used the time to 4-fold increase in starting tumor volume (RTV^4) as the experimental endpoint, with treatment effects assessed by log-rank test (evo vs. control vehicle, evo + RT vs. RT alone). Cohort sizes were 6–7 animals per group for UT-SCC-54C and 7–8 animals per group for UT-SCC-110B. Representative H&E and pimonidazole (pimo) immunostains are shown for each model. Hypoxic fractions relative to the Hoechst 33258–positive (H33258-positive) tumor area are expressed as the mean ± SEM of whole sections from 4 tumors per model. Scale bars: 50 μm (H&E) and 500 μm (pimonidazole). HR, hazard ratio.

Discussion

Systemic drugs that interact favorably with radiotherapy and immunotherapy are needed for HNSCC and other malignancies. We show that evofosfamide provides promise in this context by targeting hypoxic tumor cell populations that are refractory to radiation (2) and T cell–directed therapy (24), though varying the administered doses of these agents would be necessary to establish whether effects are synergistic or additive. The initial clinical activity and efficacy seen in tumor models (which showed hypoxic fractions comparable to clinical disease; ref. 58) establish compelling evidence for clinical development of evofosfamide in HPV-negative HNSCC. Attractive indications in the current treatment landscape include evofosfamide in combination with PD-1 blockade for platinum-resistant disease, with salvage radiation for locally recurrent disease or with first-line chemoradiation. Our observation that evofosfamide reduces hypoxia in nodal lesions is consistent

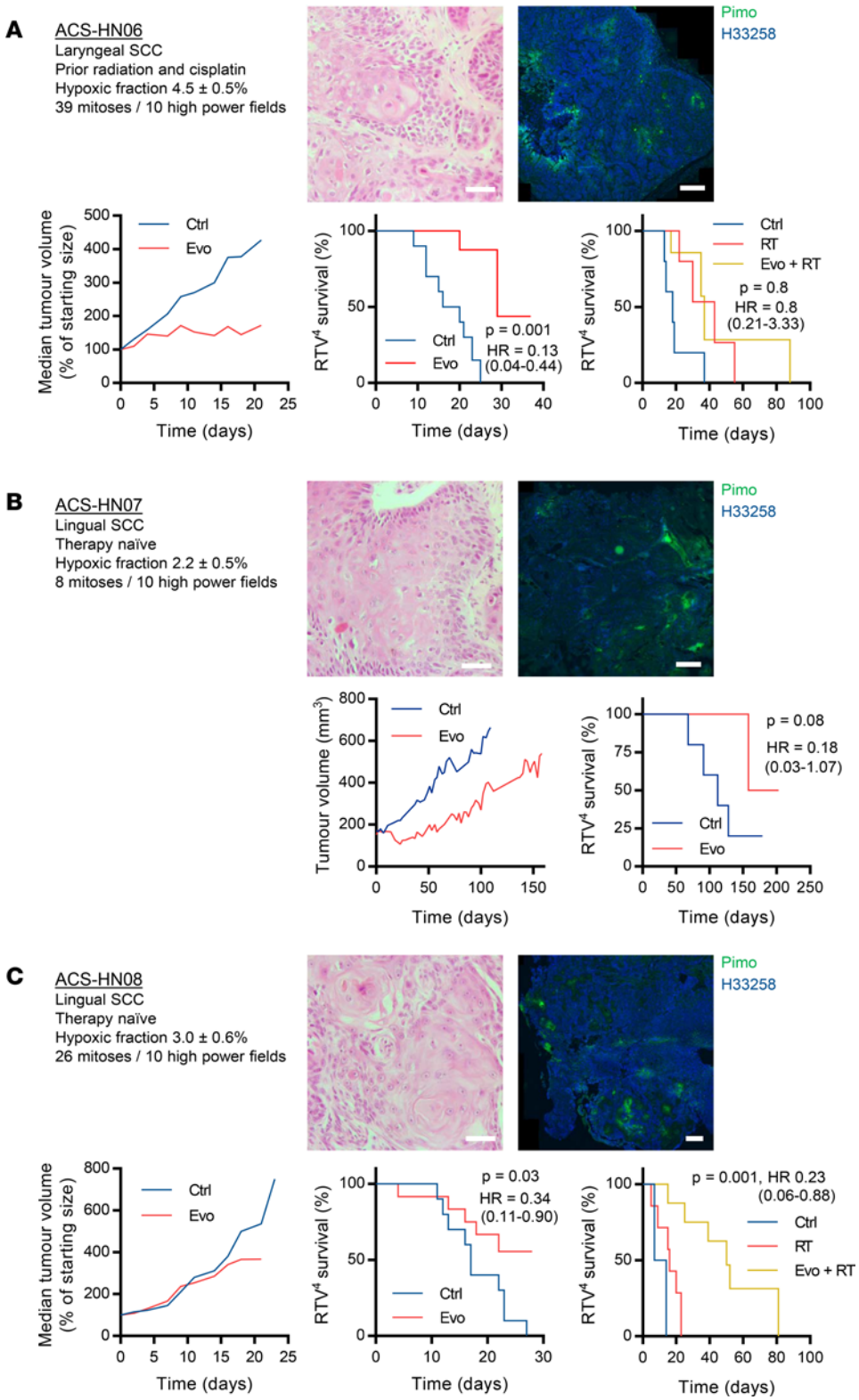

Figure 6. Efficacy of evofosfamide alone or with radiotherapy in head and neck squamous cell carcinoma (HNSCC) patient-derived xenograft models. Evofosfamide (evo) was assessed as a single agent (50 mg/kg i.p. qd × 5 weekly for 3 cycles) or in combination with radiotherapy (RT, 1 × 10 Gy on day 5 of the first cycle) by growth delay in the laryngeal patient-derived xenograft (PDX) ACS-HN06 (**A**) and the lingual PDXs ACS-HN07 (**B**) and ACS-HN08 (**C**). The patient from whom ACS-HN06 was derived had received prior radiotherapy and high-dose cisplatin, whereas ACS-HN07 and ACS-HN08 were therapy-naive. Growth plots show the volume of the median tumor at each assessment. Survival analyses used the time to 4-fold increase in starting tumor volume (RTV^4) as the experimental endpoint, with treatment effects assessed by log-rank test (evo vs. control vehicle [ctrl], evo + RT vs. RT alone). Cohort sizes were 7–10 per group. Representative H&E and pimonidazole (pimo) immunostains are shown for each model. Hypoxic fractions relative to the Hoechst 33258–positive (H33258-positive) tumor area are expressed as the mean ± SEM of whole sections from 4–7 tumors per model. The number of mitotic cells per 10 high-power fields was scored by a consultant pathologist (DK). Scale bars: 50 μm (H&E) and 500 μm (pimo). SCC, squamous cell carcinoma; HR, hazard ratio.

with the possibility of using this agent for locally advanced HNSCC presentations (such as extracapsular disease), though it will be important to confirm our observation using a more direct measure of tumor hypoxia than CA9. While combining evofosfamide with radiotherapy or chemoradiation enjoys a strong scientific rationale, the dose-limiting mucositis of evofosfamide at the monotherapy maximum tolerated dose (MTD) portends a toxicological interaction with oral/neck irradiation, as one-third of HNSCC patients treated with

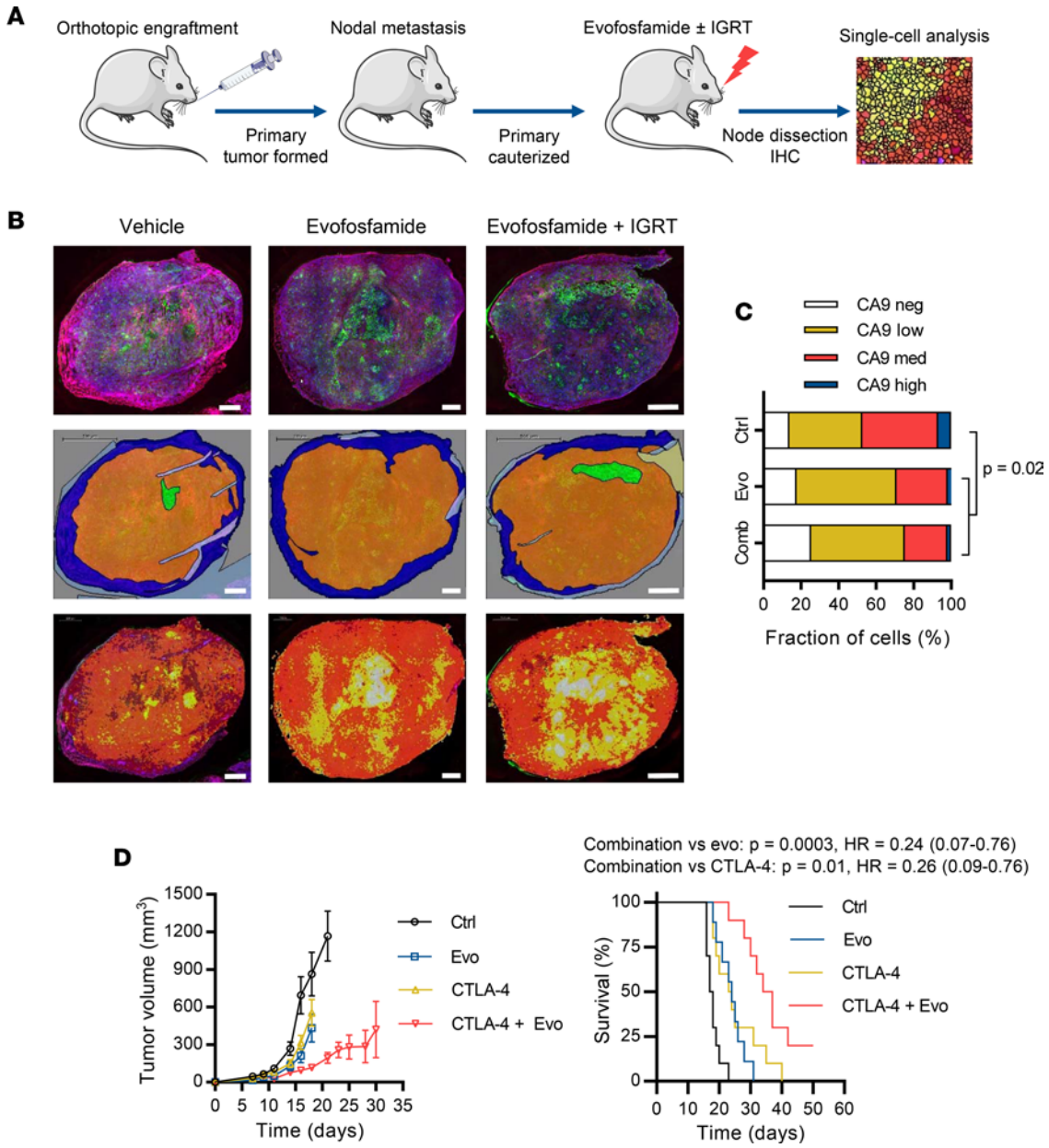

Figure 7. Evofosfamide reduces nodal hypoxia and augments CTLA-4 blockade in head and neck squamous cell carcinoma (HNSCC) tumor models. (**A**) Experimental design for assessing target engagement (as a reduction in the CA9-positive hypoxic tumor cell fraction) in nodal lesions disseminated from an orthotopic UT-SCC-74B tumor model. (**B**) Definiens TissueStudio analysis of CA9 staining in nodal lesions from treated and control animals. The top row shows CA9 staining (red), pan-cytokeratin staining (green), and DAPI staining (blue) in representative sections from each treatment group. The middle row shows tissue segmentation into tumor (orange), normal tissue (blue), necrosis (green), and artifact (gray). The bottom row shows the cellular classification, in which individual cells (identified by DAPI staining) are assigned 1 of 4 categories according to CA9 expression: negative (white), low (yellow), medium (orange), or high (red). Scale bars: 200 μm. (**C**) Comparison of the proportion of viable tumor cells showing negative, low, medium, or high expression of CA9 in nodal lesions dissected from animals treated with control vehicle (n = 2), evofosfamide monotherapy (evo, n = 3), or evofosfamide plus image-guided radiotherapy (IGRT; comb, combination n = 3) was analyzed using machine learning in the Definiens TissueStudio environment. Statistical significance of the reduction in CA9 staining in treated tumor sections was assessed by χ^2 test. (**D**) Efficacy of evofosfamide (50 mg/kg i.p. qd × 5 weekly for 2 cycles interspaced by 1-week treatment holiday) alone or with concurrent anti–CTLA-4 antibody (9H10, 100 μg/dose i.p. q3d × 3 weekly) in the syngeneic HNSCC model, SCC-7. The tumor growth plot (left panel) shows the mean ± SEM tumor volume for 10 animals per treatment group. Survival analysis (right panel) used log-rank tests with time to tumor volume ≥1,000 mm^3 to define events. HR, hazard ratio.

fractionated radiotherapy experience grade 3/4 mucositis (59). Whether dose reduction (the evofosfamide dose used with gemcitabine in the phase 3 MAESTRO trial (41) was 40% lower than monotherapy MTD) or non–concurrent scheduling can ameliorate such toxicity warrants investigation. Evofosfamide treatment has been reported to inhibit suppressive myeloid activity and enhance T cell infiltration in syngeneic tumor mod-

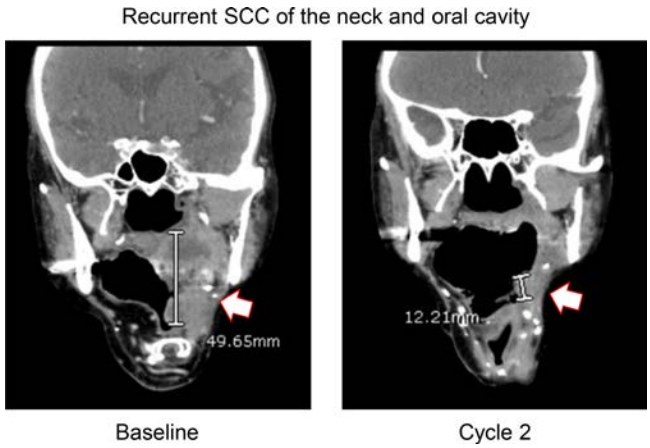

Figure 8. Partial response (PR) to evofosfamide monotherapy in an example head and neck squamous cell carcinoma (HNSCC) case. This 71-year-old woman presented with a recurrent, poorly differentiated squamous cell carcinoma (SCC) of the neck and oral cavity metastatic to lymph nodes that was previously treated with cetuximab, radiotherapy, and surgery. At baseline, the coronal CT (left panel) shows recurrent tumor centered in the left oropharynx, extending from the region of the palate to the lateral and posterior pharyngeal wall, with inferior extension into the hypopharynx. The patient received evofosfamide (480 mg/m^2 qw × 3 per 28-day cycle), with PR noted at cycles 2 (right panel) and 4. Disease progression based on target lesions was observed at cycle 6.

els (60, 61), suggesting that immunotherapy combinations may be attractive. Considering the well-described role for CTLA-4 blockade in enhancing T cell priming (62) and recent reports of synergy between CTLA-4 blockade and T cell mobilization following immunogenic nitrogen mustard–based chemotherapy in cutaneous melanoma (63), combining evofosfamide with anti–CTLA-4 antibodies may be particularly tractable. A current phase 1b trial of evofosfamide with ipilimumab, recruiting patients with defined solid tumors including HPV-negative HNSCC (NCT03098160), will provide an initial view of the safety and efficacy profile of an evofosfamide–immunotherapy combination. Given the role of hypoxia in TAM and myeloid-derived suppressor cell (MDSC) survival and recruitment (29, 31, 32), combining evofosfamide with emerging myeloid-targeted modalities, such as CSF1R inhibitors (64), may also yield therapeutic synergy.

Evofosfamide has been the subject of 26 clinical trials, most notably failing in 2 phase 3 studies — in combination with doxorubicin for unresectable or metastatic soft-tissue sarcoma (SARC021 trial) and with gemcitabine for first-line treatment of unresectable or metastatic pancreatic adenocarcinoma (PDAC; MAESTRO trial). While SARC021 was definitively negative (65) — potentially owing in part to unanticipated antagonism between evofosfamide and doxorubicin caused by intermolecular electron transfer (66) — MAESTRO only narrowly missed primary endpoint (P = 0.059 for OS) (41). Interestingly, recent data show that an ethanol-based formulation newly implemented for MAESTRO resulted in unexpected pharmacokinetics of evofosfamide, with systemic exposure at the 340 mg/m^2 MAESTRO dose equivalent to those achieved at 240 mg/m^2 in the preceding randomized phase 2 PDAC trial (53, 67). Oncologic outcomes were also consistent between the 2 cohorts (median OS 8.7 months in both cases) and these findings may explain why the efficacy seen at 340 mg/m^2 in the phase 2 trial were not reproduced in MAESTRO. Additionally, a recent retrospective molecular analysis of MAESTRO (68), in which evaluable tissue was divided into training (n = 12) and test sets (n = 172) to define a 20-protein predictive biomarker, suggested that MAESTRO would have succeeded with patient stratification when the impact of the biomarker was simulated 1,000 times across the full study cohort (n = 693). These observations suggest that evofosfamide may well be an active agent despite its clinical setbacks, given appropriate dosing and patient stratification strategies.

Failure of the prototypical hypoxic cytotoxin, tirapazamine, to extend OS with chemoradiation in HNSCC unselected for hypoxia or HPV status (23), despite evidence of specific activity in hypoxic (69), HPV-negative tumors (70), also underscores the importance of precision medicine strategies for evofosfamide (71). Using correlative and functional genomic approaches, we demonstrated evofosfamide sensitivity in HNSCC models to be associated with a proliferation-related transcriptional program, though the predictive utility of this metagene is yet to be formally defined in an independent validation setting. The latter is particularly important given our observation that the ACS-HN08 PDX model showed benefit from the addition of evofosfamide to radiotherapy, whereas ACS-HN06 did not, which could not be

explained by differences in hypoxic fraction or mitotic count. The need for independent validation notwithstanding, the fact that gene expression signatures of proliferation and hypoxia have been associated with adverse prognosis (72–74) is significant insofar as it defines a rational target population for evofosfamide. While severely hypoxic cells themselves undergo cell cycle arrest, the single-agent efficacy of evofosfamide we observed implies that this agent has substantial activity outside this severely hypoxic fraction. However, intratumor heterogeneity in proliferation- and hypoxia-related gene expression revealed by single-cell RNAseq in HNSCC (75), in addition to the known macroregional heterogeneity in hypoxia in many cancers (76), demands caution in the development of companion diagnostics that require tissue sampling. In this regard, functional imaging of tumor hypoxia such as positron emission tomography using fluorinated 2-nitroimidazole radiopharmaceuticals (77) remains attractive, with progressive improvements in this technology yielding better reproducibility, signal intensity, and resolution (78). Intriguingly, while specific prodrug-activating reductases were a dominant sensitivity modifier for tirapazamine analogues (79), this was not observed in the present study, suggesting that differences in prodrug activation (outside of hypoxia) may be smaller for evofosfamide. Notably, patients in the phase 1/2 evofosfamide monotherapy trial were not consented for genomic analysis; thus, it will be of interest to prospectively evaluate whether the biomarkers explored here are predictive of clinical benefit in HNSCC. The findings reported in the present study provide a strong rationale for the ongoing clinical development of this agent.

Methods

Compounds. Evofosfamide and Br-IPM were gifted by Threshold Pharmaceuticals. SN30000, PR-104A, and deuterated standards were synthesized at the University of Auckland, New Zealand. Cisplatin, 5-fluorouracil, and 6-thioguanine were procured from Sigma-Aldrich. Hamster anti–mouse CTLA-4 antibody (clone 9H10) was acquired from Bio X Cell. Pimonidazole was purchased from NPI Inc.

Cell lines and culture. SCC-4, SCC-9, and FaDu were sourced from the American Type Culture Collection). SCC-7 was gifted by Duska Separovic (Wayne State University, Detroit, Michigan, USA). UT-SCC cell lines were derived by Reidar Grénman at the University of Turku, Finland and short-tandem repeat (STR) profiles established in-house (Supplemental Table 3). Cells were cultured at 37°C in humidified 5% CO_2 incubators using media described in Supplemental Table 4. Cultures were maintained for less than 3 months cumulative passage from frozen stocks authenticated by STR profiling (DNA Diagnostics) and confirmed to be *Mycoplasma* negative by PlasmoTest (InvivoGen). Cell lines were confirmed HPV negative by aligning RNAseq reads to the HPV *E6* and *E7* genes. Ploidy of cell lines was measured as described in Supplemental Methods 1.1.

RNAseq. RNA was extracted from cell lines in logarithmic growth under ambient oxygen and TruSeq Stranded mRNA libraries were then prepared from 500 ng input RNA using v4 chemistry. PCR enrichment was limited to 10 cycles. Final libraries were quantified using a Qubit HS DNA Assay Kit (Thermo Fisher Scientific) and quality was assessed with a 2100 Bioanalyzer (Agilent Technologies). Libraries were normalized, pooled equimolarly, and sequenced on 3 lanes of a HiSeq 2500 flow cell with 125-bp paired-end sequencing (Illumina). Reads were aligned to hg19 with STAR and mRNA abundance estimated using RSEM. FPKM data were $\log_2$ transformed and comparison of count distributions demonstrated that further between-library normalization was unnecessary (Supplemental Figure 8). Differential expression analysis, correlation with IC_{50} data, and hierarchical clustering were performed in *R* and used *limma*, Spearman, and the ward.D method with Euclidean distance. Statistical enrichment of gene ontology (GO) and pathway classifications was assessed using the PANTHER (80) and GeneSetDB (81) databases, respectively. RNAseq data are available from the NCBI Sequence Read Archive (accession number PRJNA477597).

Whole-exome sequencing. Genomic DNA was extracted from early-passage cells using a QIAamp DNA Blood Mini Kit (Qiagen) and assessed electrophoretically and by Qubit high-sensitivity double-stranded DNA assay (Thermo Fisher Scientific). Exome libraries were prepared from 1 μg DNA using the SureSelect^{XT2} system (Agilent Technologies) with v4 chemistry following the manufacturer's protocol and sequenced on a NextSeq500 (Illumina) using high-output, 2 × 150 bp flow cells. Reads were aligned to hg19 using BWA-MEM with default parameters and variants called using VarScan-2 mpileup2snp/indel specifying maximum depth 500, mapping quality ≥15, base quality ≥10, coverage ≥20, reads2 ≥4, and variant frequency ≥0.1. The resulting vcf files were annotated using ANNOVAR, including annotation with the ljb26 ANNOVAR gene position annotations and COSMIC v81. Variants of interest were then filtered using the following criteria: (a) read depth (reference + alternate) at the variant site ≥50, (b) ≥10 reads alternate, (c) ≥20% of reads alternate, (d) the site of mutation not within the Encode Dac Mappability blacklist, (e) variant is exonic (mRNA or

ncRNA) or splicing, and (f) single-nucleotide variations not synonymous. Variants were considered of interest when less frequent than 1:1,000 in healthy humans (gnomAD exome) and either (a) predicted deleterious by PROVEAN or SIFT and the variant position was mutated in ≥1 tumor in COSMIC v81 or (b) noted as pathogenic in ClinVar by at least one investigator. Further annotations were added using the solid tumor dataset for curation of potential driver mutations in Cancer Genome Interpreter (cancergenomeinterpreter.org). Exome sequencing data are available from the NCBI Sequence Read Archive (accession number PRJNA477597).

Antiproliferative (IC_{50}) assays. Cells in logarithmic growth were seeded in 96-well plates, using densities optimized for linear dynamic range (Supplemental Table 5), and allowed to attach over 2 hours. Three-fold dilutions of compounds (10 increments in duplicate per compound) were then added to the plates and incubated for 4 hours prior to wash-out effected by 3 media changes. For anoxic treatments, cells were plated, attached, and treated in an H_2/Pd-scrubbed HEPA Hypoxystation (Don Whitley Scientific) using media and plasticware equilibrated for ≥3 days. The plates were then incubated in 20% oxygen for 5 days before assessing culture density by sulforhodamine B colorimetry. Four-parameter logistic regressions were fitted to the concentration-response curves and solved to compute IC_{50} values, which were defined as drug concentrations that reduced cell number to 50% of untreated wells on the same plate.

LC-MS/MS assays of evofosfamide metabolism. Cells were prepared for drug metabolism studies and intracellular and extracellular samples were extracted with methanol, pooled, and evofosfamide, Br-IPM, Cl-IPM, and Tr-H were analyzed by LC-MS/MS as reported (82).

Whole-genome CRISPR knockout screens. Whole-genome CRISPR knockout screens for modifiers of sensitivity to evofosfamide and Br-IPM in UT-SCC-74B were performed as described in Supplemental Methods 1.2.

CDX models. Age-matched, female NIH-III mice (NIH-*Lyst*$^{bg\text{-}J}$*Foxn1*^{nu}*Btk*^{xid}; Charles River) were inoculated with 5 × 10^6 UT-SCC-110B or UT-SCC-54C cells subcutaneously into the spinal midline 10 mm above the tail base. Tumor volume was monitored by electronic calipers using the function π/6 × width × length^2. Once tumors reached 200 mm^3, they were randomized to receive control vehicle (saline), 50 mg/kg evofosfamide, saline with 10 Gy radiation, or 50 mg/kg evofosfamide with 10 Gy radiation. Evofosfamide and saline were administered i.p. qd × 5 for 3 weekly cycles. Radiation was administered on day 5 of cycle 1 locally to the tumor while animals were restrained and shielded in a custom-designed jig and using a ^{60}Co Eldorado 78 radiotherapy unit at a dose rate of 1.7 Gy/min. Hypoxic fractions of CDX models were assessed as described in Supplemental Methods 1.4.

PDX models. Fresh tumor specimens were obtained from resections performed at Auckland City Hospital of histologically confirmed HNSCC presumed HPV-negative by p16 immunostaining and extraoropharyngeal primary site. Tissue was engrafted into anesthetized (100 mg/kg ketamine, Ceva Animal Health; 10 mg/kg xylazine, Phoenix Pharm), 6- to 8-week old, female NSG (NOD.Cg-*Prkdc*^{scid}*Il2rγ*^{tm1Wjl}/SzJ; Jackson Laboratory) or NOD scid (NOD.CB17-*Prkdc*^{scid}/NCrCrl; Charles River) mice as 1- to 2-mm^3 fragments through an incision on bilateral subcutaneous flanks. Upon reaching 1,500 mm^3, tumors were fragmented and collected for cryopreservation or engraftment into additional mice. Second-generation PDXs were grown to 1,500 mm^3, and then the mice were treated i.p. with 60 mg/kg pimonidazole and tumors collected for histology, DNA extraction, or subcutaneous engraftment on the midline (as above) for radiotherapy or bilaterally on the flanks for evofosfamide monotherapy. NIH-III mice with third-generation PDXs were randomized to receive drug treatment as above once tumors reached 200 mm^3. Targeted sequencing of 409 genes using the Ion AmpliSeq Comprehensive Cancer Panel (Thermo Fisher Scientific) was performed for the PDX models and originating clinical specimens as described in Supplemental Methods 1.3. Histopathological characterization of the PDX models is described in Supplemental Information Section 4. Hypoxic fractions of PDX models were assessed as described in Supplemental Methods 1.4.

Orthotopic model. UT-SCC-74B cells (0.5 × 10^6 in 30 μl) were injected into the tongue tip of female, 8- to 12-week-old NSG mice and palpable tumors resected thereafter under anesthesia (5% isoflurane induction; 2% maintenance). For analgesia, 5 mg/kg meloxicam and 0.1 mg/kg buprenorphine (both s.c.) were administered before surgery, then meloxicam was given qd × 2. Once the animals reached the surgical plane, tumors were removed using a microvessel cauterization tool. Enrofloxacin (2.27 mg/ml) was administered in drinking water for 7 days after surgery and animals were weighed regularly. Twelve days after resection, animals were randomized to receive evofosfamide alone or in combination with cervical lymph node irradiation delivered using an X-RAD 320 image-guided radiotherapy unit (Precision X-Ray). Evofosfamide was administered i.p. at 50 mg/kg qd × 5 in saline in a weekly schedule for 13 doses. Beginning on the same day, radiation was delivered as 3 × 2 Gy daily fractions to anesthetized (isoflurane as above)

mice in 2 lateral beams directed at the cervical lymph nodes using an 8-mm collimator and a dose rate of 2.53 Gy/min calculated for an isocentric depth of 6 mm. Six days after completing treatment, mice were administered 1 mg i.v. H33258 (Sigma-Aldrich) and nodal tumors harvested for CA9 and pan-cytokeratin immunohistochemistry, imaging, and quantification as described in Supplemental Methods 1.5.

Syngeneic model. SCC-7 cells (10^5, ATCC) were engrafted in the right flank subcutis of female, 6- to 8-week-old C3H/HeJ (*Tlr4*$^{Lps\text{-}d}$) mice (Jackson Laboratory). Beginning 7 days after inoculation, evofosfamide was administered i.p. at 50 mg/kg qd × 5 for 2 weekly cycles spaced by a 1-week treatment holiday. Concurrent αCTLA-4 (9H10, Bio X Cell) was administered i.p. at 100 μg/dose on days 1, 4, and 7 of each cycle. Tumor growth was monitored by electronic calipers as above and events for survival analysis (log-rank test) recorded when tumors reached 1,000 mm^3.

Clinical evaluation. Five patients with unresectable or metastatic, histologically confirmed HNSCC who had failed standard of care were recruited, with informed consent, to a phase 2, multicenter, open-label, nonrandomized solid tumor dose expansion cohort to a phase 1a evofosfamide monotherapy trial (NCT00495144). The dose-escalation phase of the trial, which recruited 57 patients and defined dose-limiting toxicities and an evofosfamide MTD of 575 mg/m^2 as 30- to 60-minute i.v. infusion administered on days 1, 8, and 15 of 28-day cycles, has already been published (52). Patients in the unpublished phase 2 expansion cohort, which recruited 72 subjects with malignant melanoma, small-cell lung cancer, non–small-cell lung cancer, hepatocellular carcinoma, or malignancies with squamous or transitional cell histology, received evofosfamide at 575 mg/m^2 or 480 mg/m^2 using the same treatment schedule. Inclusion criteria were age ≥18 years, measurable disease by RECIST 1.0, Eastern Cooperative Oncology Group (ECOG) performance status of 0 or 1, resolution of reversible toxicity from prior therapies, serum creatinine at or below the upper limit of normal, and adequate liver and hematologic function. Prior high-dose chemotherapy or radiotherapy to >25% of the bone marrow were exclusion criteria. All 5 HNSCC who were recruited had progressed locally or distantly after prior surgery and fractionated radiotherapy with concurrent cisplatin or cetuximab. These subjects received up to 6 cycles of evofosfamide at 480 mg/m^2, with further cycles available at the discretion of the investigator. The primary endpoint was objective response rate (ORR, per RECIST 1.0 assessed at each cycle), while PFS and duration of response were secondary endpoints. Toxicity was graded according to the National Cancer Institute Common Toxicity Criteria for Adverse Events (NCI CTCAE) version 3.0.

Statistics. Statistical tests were performed in *R*, Prism (v7.03; GraphPad) or SigmaPlot (v13.0; Systat Software) and were 2-tailed. Two-tailed Student's *t* tests, Mann-Whitney tests, and 1-way ANOVA with Dunnett's correction were used for assessment of differences between 2 or more groups, respectively, except for differences in CA9 staining, which were assessed by χ^2 test with integer-rounded percentages. Linear regression analysis used Pearson's correlation testing. Differential expression analyses used the *limma* method, with gene expression clusters generated using the ward.D method with Euclidean distance. Enrichment of gene ontology and molecular pathway terms in gene lists were assessed using Fisher's exact tests. Adjustment for multiple hypothesis testing used the Benjamini–Hochberg method. Survival analyses used log-rank tests with events defined as a 4-fold increase in tumor volume from baseline (CDX and PDX models) or time to 1,000-mm^3 tumor volume (SCC-7). *P* values less than 0.05 were considered significant. Animal experiments were randomized and nonblinded. In all box-and-whisker plots, boxes denote the median, interquartile range, and minimum and maximum observations from independent replication of experiments. Replicate numbers and details of statistical tests used are described in the figure legends.

Study approvals. The clinical study was performed after institutional review boards' approval and in accord with assurances filed with and approved by the U.S. Department of Health and Human Services. The collection of patient specimens for PDX engraftment was approved by the New Zealand Health and Disability Ethics Committee and Auckland City Hospital. Written informed consent was received from all participants prior to their inclusion in the clinical study of for collection of tumor tissue. All animal experiments observed institutional guidelines at the University of Auckland, Princess Margaret Centre and MD Anderson Cancer Center, and in accord with animal welfare laws in New Zealand, Canada, and the United States.

Author contributions

SMFJ, MKK, TDM, KOH, SKB, BGW, CPH, WRW, MAC, and FWH designed and supervised experiments. PB, AL, AS, WWW, DL, PMK, CRHL, CRH, TWL, LC, MZ, SB, and FWH performed experiments and collected experimental data. SMFJ, PT, DK, NPL, PMK, NSK, CRH, TWL, TDM, KOH,

CGP, MAC, and FWH analyzed experimental and/or bioinformatic data. NNS, EGC, SIJ, JJN, DK, AMJM, NPM, and JMC consented patients, treated patients, and provided tissue samples. SMFJ, SKB, BGW, CPH, CGP, WRW, and FWH conceived and led the study. RAG developed the UT-SCC cell lines. All authors contributed to writing and editing the manuscript.

Acknowledgments

The authors are grateful to the patients and their families who participated in this research through clinical trial involvement or tissue donation. We thank New Zealand Genomics Ltd. for RNAseq services, Emma Wrightson for the generation of PDX models, Michael Hay and Benjamin Dickson for drug synthesis, Sarah McManaway and Julia Harms for STR profiling and the quantification of hypoxic fractions in PDX models, Umaiyaall Shanmugaraajah for the measurement of cell line doubling times, and Chandrakanth Bhoothpur for the targeted sequencing of PDX models. Assistance from the Auckland Regional Tissue Bank is gratefully acknowledged. This work was supported by the Cancer Research Trust New Zealand (John Gavin Postdoctoral Fellowship GOT-1438-JGPDF to F.W. Hunter); the Cancer Society of New Zealand (project grant 15.16 to F.W. Hunter, W.R. Wilson, and C.G. Print); the Health Research Council of New Zealand (Programme grant 14/538 to W.R. Wilson, S.M.F. Jamieson, K.O. Hicks, and C.G. Print); the Maurice Wilkins Centre for Molecular Biodiscovery (specialized equipment access grants to F.W. Hunter and S.M.F. Jamieson); Threshold Pharmaceuticals, Inc. (commercial sponsorship of clinical trial NCT00495144); the University of Auckland (early-career research excellence award to F.W. Hunter and Biopharma Thematic Research Initiative to S.M.F. Jamieson); the Royal Society Te Apārangi (Marsden grant UOA1401 to W.R. Wilson, S.K. Bohlander, F.W. Hunter, and C.G. Print); and the MD Anderson Stiefel Oropharyngeal Research Fund (to M.A. Curran). P.M. Kakadia and S.K. Bohlander were supported by Leukaemia & Blood Cancer New Zealand and the family of Marijanna Kumerich.

Address correspondence to: Francis W. Hunter, Auckland Cancer Society Research Centre, University of Auckland, 85 Park Road, Grafton, Auckland, New Zealand. Phone: 64.923.6710; Email: f.hunter@auckland.ac.nz.

1. Wilson WR, Hay MP. Targeting hypoxia in cancer therapy. *Nat Rev Cancer*. 2011;11(6):393–410.
2. Nordsmark M, et al. Prognostic value of tumor oxygenation in 397 head and neck tumors after primary radiation therapy. An international multi-center study. *Radiother Oncol*. 2005;77(1):18–24.
3. Brizel DM, Sibley GS, Prosnitz LR, Scher RL, Dewhirst MW. Tumor hypoxia adversely affects the prognosis of carcinoma of the head and neck. *Int J Radiat Oncol Biol Phys*. 1997;38(2):285–289.
4. Lassen P, et al. HPV-associated p16-expression and response to hypoxic modification of radiotherapy in head and neck cancer. *Radiother Oncol*. 2010;94(1):30–35.
5. Ferlay J, et al. Cancer incidence and mortality worldwide: sources, methods and major patterns in GLOBOCAN 2012. *Int J Cancer*. 2015;136(5):E359–E386.
6. Blot WJ, et al. Smoking and drinking in relation to oral and pharyngeal cancer. *Cancer Res*. 1988;48(11):3282–3287.
7. Gillison ML, et al. Evidence for a causal association between human papillomavirus and a subset of head and neck cancers. *J Natl Cancer Inst*. 2000;92(9):709–720.
8. Agrawal N, et al. Exome sequencing of head and neck squamous cell carcinoma reveals inactivating mutations in NOTCH1. *Science*. 2011;333(6046):1154–1157.
9. Stransky N, et al. The mutational landscape of head and neck squamous cell carcinoma. *Science*. 2011;333(6046):1157–1160.
10. Partlová S, et al. Distinct patterns of intratumoral immune cell infiltrates in patients with HPV-associated compared to non-virally induced head and neck squamous cell carcinoma. *Oncoimmunology*. 2015;4(1):e965570.
11. Ang KK, et al. Human papillomavirus and survival of patients with oropharyngeal cancer. *N Engl J Med*. 2010;363(1):24–35.
12. Fakhry C, et al. Improved survival of patients with human papillomavirus-positive head and neck squamous cell carcinoma in a prospective clinical trial. *J Natl Cancer Inst*. 2008;100(4):261–269.
13. Cooper JS, et al. Postoperative concurrent radiotherapy and chemotherapy for high-risk squamous-cell carcinoma of the head and neck. *N Engl J Med*. 2004;350(19):1937–1944.
14. Adelstein DJ, et al. An intergroup phase III comparison of standard radiation therapy and two schedules of concurrent chemoradiotherapy in patients with unresectable squamous cell head and neck cancer. *J Clin Oncol*. 2003;21(1):92–98.
15. Ozanne B, Richards CS, Hendler F, Burns D, Gusterson B. Over-expression of the EGF receptor is a hallmark of squamous cell carcinomas. *J Pathol*. 1986;149(1):9–14.
16. Bonner JA, et al. Radiotherapy plus cetuximab for squamous-cell carcinoma of the head and neck. *N Engl J Med*. 2006;354(6):567–578.
17. Vermorken JB, et al. Platinum-based chemotherapy plus cetuximab in head and neck cancer. *N Engl J Med*. 2008;359(11):1116–1127.
18. Ferris RL, et al. Nivolumab for recurrent squamous-cell carcinoma of the head and neck. *N Engl J Med*. 2016;375(19):1856–1867.
19. Seiwert TY, et al. Safety and clinical activity of pembrolizumab for treatment of recurrent or metastatic squamous cell carcinoma of the head and neck (KEYNOTE-012): an open-label, multicentre, phase 1b trial. *Lancet Oncol*. 2016;17(7):956–965.
20. Overgaard J. Hypoxic modification of radiotherapy in squamous cell carcinoma of the head and neck--a systematic review and

meta-analysis. *Radiother Oncol*. 2011;100(1):22–32.
21. Kaanders JH, Bussink J, van der Kogel AJ. ARCON: a novel biology-based approach in radiotherapy. *Lancet Oncol*. 2002;3(12):728–737.
22. Overgaard J, et al. A randomized double-blind phase III study of nimorazole as a hypoxic radiosensitizer of primary radiotherapy in supraglottic larynx and pharynx carcinoma. Results of the Danish Head and Neck Cancer Study (DAHANCA) Protocol 5-85. *Radiother Oncol*. 1998;46(2):135–146.
23. Rischin D, et al. Tirapazamine, cisplatin, and radiation versus cisplatin and radiation for advanced squamous cell carcinoma of the head and neck (TROG 02.02, HeadSTART): a phase III trial of the Trans-Tasman Radiation Oncology Group. *J Clin Oncol*. 2010;28(18):2989–2995.
24. Chouaib S, Noman MZ, Kosmatopoulos K, Curran MA. Hypoxic stress: obstacles and opportunities for innovative immunotherapy of cancer. *Oncogene*. 2017;36(4):439–445.
25. Noman MZ, et al. PD-L1 is a novel direct target of HIF-1α, and its blockade under hypoxia enhanced MDSC-mediated T cell activation. *J Exp Med*. 2014;211(5):781–790.
26. Ottensmeier CH, et al. Upregulated glucose metabolism correlates inversely with $CD8^+$ T-cell infiltration and survival in squamous cell carcinoma. *Cancer Res*. 2016;76(14):4136–4148.
27. Facciabene A, et al. Tumour hypoxia promotes tolerance and angiogenesis via CCL28 and T(reg) cells. *Nature*. 2011;475(7355):226–230.
28. Deng B, et al. Intratumor hypoxia promotes immune tolerance by inducing regulatory T cells via TGF-β1 in gastric cancer. *PLoS ONE*. 2013;8(5):e63777.
29. Lewis C, Murdoch C. Macrophage responses to hypoxia: implications for tumor progression and anti-cancer therapies. *Am J Pathol*. 2005;167(3):627–635.
30. Lewis CE, Pollard JW. Distinct role of macrophages in different tumor microenvironments. *Cancer Res*. 2006;66(2):605–612.
31. Corzo CA, et al. HIF-1α regulates function and differentiation of myeloid-derived suppressor cells in the tumor microenvironment. *J Exp Med*. 2010;207(11):2439–2453.
32. Doedens AL, et al. Macrophage expression of hypoxia-inducible factor-1 alpha suppresses T-cell function and promotes tumor progression. *Cancer Res*. 2010;70(19):7465–7475.
33. Ohta A, et al. A2A adenosine receptor protects tumors from antitumor T cells. *Proc Natl Acad Sci USA*. 2006;103(35):13132–13137.
34. Lardner A. The effects of extracellular pH on immune function. *J Leukoc Biol*. 2001;69(4):522–530.
35. Nakagawa Y, Negishi Y, Shimizu M, Takahashi M, Ichikawa M, Takahashi H. Effects of extracellular pH and hypoxia on the function and development of antigen-specific cytotoxic T lymphocytes. *Immunol Lett*. 2015;167(2):72–86.
36. Payen VL, Porporato PE, Baselet B, Sonveaux P. Metabolic changes associated with tumor metastasis, part 1: tumor pH, glycolysis and the pentose phosphate pathway. *Cell Mol Life Sci*. 2016;73(7):1333–1348.
37. Duan JX, et al. Potent and highly selective hypoxia-activated achiral phosphoramidate mustards as anticancer drugs. *J Med Chem*. 2008;51(8):2412–2420.
38. Saggar JK, Tannock IF. Activity of the hypoxia-activated pro-drug TH-302 in hypoxic and perivascular regions of solid tumors and its potential to enhance therapeutic effects of chemotherapy. *Int J Cancer*. 2014;134(11):2726–2734.
39. Meng F, et al. Molecular and cellular pharmacology of the hypoxia-activated prodrug TH-302. *Mol Cancer Ther*. 2012;11(3):740–751.
40. Sun JD, et al. Selective tumor hypoxia targeting by hypoxia-activated prodrug TH-302 inhibits tumor growth in preclinical models of cancer. *Clin Cancer Res*. 2012;18(3):758–770.
41. Van Cutsem E, et al. MAESTRO: A randomized, double-blind phase III study of evofosfamide (Evo) in combination with gemcitabine (Gem) in previously untreated patients (pts) with metastatic or locally advanced unresectable pancreatic ductal adenocarcinoma (PDAC). *J Clin Oncol*. 2016;34(15_suppl):4007.
42. Liu Q, et al. TH-302, a hypoxia-activated prodrug with broad in vivo preclinical combination therapy efficacy: optimization of dosing regimens and schedules. *Cancer Chemother Pharmacol*. 2012;69(6):1487–1498.
43. Duran R, et al. Preclinical benefit of hypoxia-activated intra-arterial therapy with evofosfamide in liver cancer. *Clin Cancer Res*. 2017;23(2):536–548.
44. Peeters SG, et al. TH-302 in combination with radiotherapy enhances the therapeutic outcome and is associated with pretreatment [18F]HX4 hypoxia PET imaging. *Clin Cancer Res*. 2015;21(13):2984–2992.
45. Hu J, et al. Synergistic induction of apoptosis in multiple myeloma cells by bortezomib and hypoxia-activated prodrug TH-302, in vivo and in vitro. *Mol Cancer Ther*. 2013;12(9):1763–1773.
46. Portwood S, et al. Activity of the hypoxia-activated prodrug, TH-302, in preclinical human acute myeloid leukemia models. *Clin Cancer Res*. 2013;19(23):6506–6519.
47. Hunter FW, Hsu HL, Su J, Pullen SM, Wilson WR, Wang J. Dual targeting of hypoxia and homologous recombination repair dysfunction in triple-negative breast cancer. *Mol Cancer Ther*. 2014;13(11):2501–2514.
48. Lohse I, et al. Targeting hypoxic microenvironment of pancreatic xenografts with the hypoxia-activated prodrug TH-302. *Oncotarget*. 2016;7(23):33571–33580.
49. Benito J, et al. Hypoxia-activated prodrug TH-302 targets hypoxic bone marrow niches in preclinical leukemia models. *Clin Cancer Res*. 2016;22(7):1687–1698.
50. Zhang L, Marrano P, Wu B, Kumar S, Thorner P, Baruchel S. Combined antitumor therapy with metronomic topotecan and hypoxia-activated prodrug, evofosfamide, in neuroblastoma and rhabdomyosarcoma preclinical models. *Clin Cancer Res*. 2016;22(11):2697–2708.
51. Nytko KJ, et al. The hypoxia-activated prodrug evofosfamide in combination with multiple regimens of radiotherapy. *Oncotarget*. 2017;8(14):23702–23712.
52. Weiss GJ, et al. Phase 1 study of the safety, tolerability, and pharmacokinetics of TH-302, a hypoxia-activated prodrug, in patients with advanced solid malignancies. *Clin Cancer Res*. 2011;17(9):2997–3004.
53. Borad MJ, et al. Randomized phase II trial of gemcitabine plus TH-302 versus gemcitabine in patients with advanced pancreatic cancer. *J Clin Oncol*. 2015;33(13):1475–1481.
54. Patterson AV, et al. Mechanism of action and preclinical antitumor activity of the novel hypoxia-activated DNA cross-linking

agent PR-104. *Clin Cancer Res*. 2007;13(13):3922–3932.
55. Hicks KO, et al. Pharmacokinetic/pharmacodynamic modeling identifies SN30000 and SN29751 as tirapazamine analogues with improved tissue penetration and hypoxic cell killing in tumors. *Clin Cancer Res*. 2010;16(20):4946–4957.
56. Sanjana NE, Shalem O, Zhang F. Improved vectors and genome-wide libraries for CRISPR screening. *Nat Methods*. 2014;11(8):783–784.
57. Nagalla S, et al. Interactions between immunity, proliferation and molecular subtype in breast cancer prognosis. *Genome Biol*. 2013;14(4):R34.
58. Wijffels KI, et al. Vascular architecture and hypoxic profiles in human head and neck squamous cell carcinomas. *Br J Cancer*. 2000;83(5):674–683.
59. Trotti A, et al. Mucositis incidence, severity and associated outcomes in patients with head and neck cancer receiving radiotherapy with or without chemotherapy: a systematic literature review. *Radiother Oncol*. 2003;66(3):253–262.
60. Ai M, et al. Tumor hypoxia drives immune suppression and immunotherapy resistance. *J Immunother Cancer*. 2015;3(Suppl_2) :P392.
61. Ai M et al. Combination hypoxia-specific chemotherapy and immunotherapy of prostate cancer. *Cancer Res*. 2014;74(19):A629.
62. Sotomayor EM, Borrello I, Tubb E, Allison JP, Levitsky HI. In vivo blockade of CTLA-4 enhances the priming of responsive T cells but fails to prevent the induction of tumor antigen-specific tolerance. *Proc Natl Acad Sci USA*. 1999;96(20):11476–11481.
63. Ariyan CE, et al. Robust antitumor responses result from local chemotherapy and CTLA-4 blockade. *Cancer Immunol Res*. 2018;6(2):189–200.
64. Cannarile MA, Weisser M, Jacob W, Jegg AM, Ries CH, Rüttinger D. Colony-stimulating factor 1 receptor (CSF1R) inhibitors in cancer therapy. *J Immunother Cancer*. 2017;5(1):53.
65. Tap WD, et al. Doxorubicin plus evofosfamide versus doxorubicin alone in locally advanced, unresectable or metastatic soft-tissue sarcoma (TH CR-406/SARC021): an international, multicentre, open-label, randomised phase 3 trial. *Lancet Oncol*. 2017;18(8):1089–1103.
66. Anderson RF, Li D, Hunter FW. Antagonism in effectiveness of evofosfamide and doxorubicin through intermolecular electron transfer. *Free Radic Biol Med*. 2017;113:564–570.
67. Higgins JP, Sarapa N, Kim J, Poma E. Unexpected pharmacokinetics of evofosfamide observed in phase III MAESTRO study. *J. Clin. Oncol*. 2018;36(15_suppl):2568.
68. Domenyuk V, et al. Poly-ligand profiling differentiates pancreatic cancer patients according to treatment benefit from gemcitabine+placebo versus gemcitabine+evofosfamide and identifies candidate targets. *Ann Oncol*. 2018;29(suppl_5):m dy151.131.
69. Rischin D, et al. Prognostic significance of [18F]-misonidazole positron emission tomography-detected tumor hypoxia in patients with advanced head and neck cancer randomly assigned to chemoradiation with or without tirapazamine: a substudy of Trans-Tasman Radiation Oncology Group Study 98.02. *J Clin Oncol*. 2006;24(13):2098–2104.
70. Rischin D, et al. Prognostic significance of p16INK4A and human papillomavirus in patients with oropharyngeal cancer treated on TROG 02.02 phase III trial. *J Clin Oncol*. 2010;28(27):4142–4148.
71. Hunter FW, Wouters BG, Wilson WR. Hypoxia-activated prodrugs: paths forward in the era of personalised medicine. *Br J Cancer*. 2016;114(10):1071–1077.
72. Zhang L, et al. Genomic analysis of nasopharyngeal carcinoma reveals TME-based subtypes. *Mol Cancer Res*. 2017;15(12):1722–1732.
73. Giri U, et al. Molecular signatures associated with clinical outcome in patients with high-risk head-and-neck squamous cell carcinoma treated by surgery and radiation. *Int J Radiat Oncol Biol Phys*. 2006;64(3):670–677.
74. Toustrup K, et al. Development of a hypoxia gene expression classifier with predictive impact for hypoxic modification of radiotherapy in head and neck cancer. *Cancer Res*. 2011;71(17):5923–5931.
75. Puram SV, et al. Single-cell transcriptomic analysis of primary and metastatic tumor ecosystems in head and neck cancer. *Cell*. 2017;171(7):1611–1624.e24.
76. Dhani NC, et al. Analysis of the intra- and intertumoral heterogeneity of hypoxia in pancreatic cancer patients receiving the nitroimidazole tracer pimonidazole. *Br J Cancer*. 2015;113(6):864–871.
77. Horsman MR, Mortensen LS, Petersen JB, Busk M, Overgaard J. Imaging hypoxia to improve radiotherapy outcome. *Nat Rev Clin Oncol*. 2012;9(12):674–687.
78. Silvoniemi A, Suilamo S, Laitinen T, Forsback S. Repeatability of tumour hypoxia imaging using [18 F]-EF5 PET/CT in head and neck cancer. *Eur J Nucl Med Mol Imaging*. 2017;45(2):161–169.
79. Hunter FW, et al. Identification of P450 oxidoreductase as a major determinant of sensitivity to hypoxia-activated prodrugs. *Cancer Res*. 2015;75(19):4211–4223.
80. Mi H, et al. PANTHER version 11: expanded annotation data from Gene Ontology and Reactome pathways, and data analysis tool enhancements. *Nucleic Acids Res*. 2017;45(D1):D183–D189.
81. Araki H, Knapp C, Tsai P, Print C. GeneSetDB: A comprehensive meta-database, statistical and visualisation framework for gene set analysis. *FEBS Open Bio*. 2012;2:76–82.
82. Hong CR, et al. Cellular pharmacology of evofosfamide (TH-302): A critical re-evaluation of its bystander effects. *Biochem Pharmacol*. In press.
83. Luo B, et al. Highly parallel identification of essential genes in cancer cells. *Proc Natl Acad Sci USA*. 2008;105(51):20380–20385.